2 TABLE LOOK-UP METHOD (Y.Knyazikhin, Y.Tian, Y.Zhang, Y.Wang and R.Myneni)

2.1. Mathematical formulation of the inverse problem

Land surface processes are important components of the terrestrial climate system. Accurate descriptions of the interaction between the surface and the atmosphere require reliable quantitative information on the fluxes, mass, and momentum, especially over terrestrial areas, where they are closely associated with the rates of evapotranspiration and photosynthesis. Many of these processes can be related to the spectral reflectance of the surface (Kimes *et al.,* 1987) (Sellers, 1985). The vegetation canopy is classified as a special type of surface not only due to its role in the energy balance but also due to its impact on the global carbon cycle (Sundquist, 1993). Its reflection results from bio-physiological, chemical and physical processes, and is characterized by spatial, seasonal and diurnal variations. Modern satellite-born sensors (e.g., MODIS, MISR, POLDER, SeaWiFS) allow for rich spectral and angular sampling of the radiation field reflected by vegetation canopies. This sets new demands on the retrieval techniques for geophysical parameters in order to fully take advantage of these instruments.

There are three attributes which, directly or indirectly, are included in any existing retrieval algorithm. They are (1) an instrument specific space D of all possible observations of canopy reflectances; (2) the space P of all possible canopy realizations encountered in reality and which are taken into account by a problem-specific retrieval technique; and (3) a relationship F between these spaces which to every element p from P sets in correspondence an element $F(p)$ from the space D.

For the sake of simplicity, we consider the use of canopy reflectances at near-infrared and red wavelengths for the retrieval techniques in this paper. Figure 1 demonstrates the distribution of vegetated pixels from the SeaWiFS data set with respect to their reflectances at near-infrared and red wavelengths. This set is an example of an instrument specific space D^* of observations of canopy reflectances. An element of this space is a vector on the NIR-RED plane which depends on the direction Ω_0 of direct solar radiance and view direction Ω. Some instruments (e.g., MISR, Diner *et al*., 1998) can also provide the ratio f_{dir} of direct radiation to the total (direct and diffuse) radiation incident on the pixel. The aim of the space D is to represent all possible observations of canopy reflectances D^* to within a certain degree of accuracy.

The three-dimensional canopy structure, and the optical properties of vegetation elements (leaves, stems) and soil are the most important variables determining the three-dimensional radiation field in vegetation canopies. We formulate the inverse problem for three-dimensional vegetation canopies: given mean spectral and angular signatures of canopy-leaving radiance averaged over the three-dimensional canopy radiation field, find desired vegetation parameters. The effective use of three-dimensional canopy radiation models, however, presuppose that three-dimensional input variables are available. Therefore any development of a radiation model should be accompanied simultaneously by a modeling of realistic patterns of these variables. Thus a data bank, containing patterns of three-dimensional environmental variables can be generated. Given such a bank one can compose various patterns of vegetation canopies encountered in reality which form the space P. Three-dimensional models of canopy architecture has been a highly active research field in recent years (Borel-Donohue, 1988) (Reffye *et al*., 1991) (Kranigk and Gravenhorst, 1993) (Chen *et al*., 1994) (Kurth, 1994) (Knyazikhin *et al*., 1996). However these models are not widely used in designing retrieval algorithms. This definition of P allows for their use in inversion techniques. Figure 2 demonstrates an example of

the architecture of individual trees. Given architectural patterns of individual trees and its distribution in the canopy one can compose the architecture of the entire canopy (Figure 3). Figure 4 demonstrates patterns of spectral leaf albedo (left) and soil reflectance (right). Thus an element $p=(\chi,\omega,\rho)$ of the space P consist of canopy structure (Figure 3, right, as χ), optical properties of leaves (a spectral curve from Figure 4, left, as ω) and soil (a spectral curve from Figure 4, right, as ρ). The more elements in space P, the more accurate this space represents canopy realizations encountered in reality.

The above definition of P was used in designing the algorithm for retrieval leaf area index (LAI) and fraction of absorbed photosynthetically active radiation (FPAR) from canopy reflectances data measured by MODIS (moderate resolution imaging spectroradiometer) and MISR (multiangle imaging spectroradiometer) instruments (Knyazikhin *et al.*, 1998a) (Knyazikhin *et al.*, 1998b). The space P was represented by six canopy structural types of global vegetation (biome) (*Myneni et al.*, 1997), each representing a pattern of the canopy structure χ(bio) and leaf optical spectra ω(bio). Each biome is characterized by ground cover g, mean LAI of an individual plant L, and pattern of ground reflectances $\rho=(\rho_1, \rho_2, \ldots, \rho_N)$ at spectral bands of the instrument (N=7 for MODIS and N=4 for MISR). The element p of this space is the vector $p=(\chi(\text{bio}), \omega(\text{bio}), \rho, L, g)$. Here the identification number bio for the biome type can take six values only; one pattern $\omega(\text{bio})=(\omega_1, \omega_2, \ldots,\omega_N)$ of the spectral leaf albedo per biome. In the case of the MODIS instrument the biome type is assumed known and serves as input for the retrieval algorithm. Ground cover and the LAI of individual plant can vary continuously within given biome-dependent ranges. The set of various patterns $\rho=(\rho_1, \rho_2, \ldots, \rho_N)$ of the ground reflectances (Figure 4, right) is a static table of the LAI/FPAR algorithm. Note that the leaf area index is not included in the vector p. However given the ground cover g and the mean LAI of an individual plant L this variable can be evaluated as $\text{LAI}(p)=gL$. If the space P is parameterized in another manner, the relationship between LAI and the vector p may take another suitable form.

The third step in designing a retrieval algorithm is to establish a relationship F between P and D. Here F is a vector $(F_{\text{RED}}(p), F_{\text{NIR}}(p))$ whose coordinates are canopy reflectances at red and near-infrared wavelengths. The photon transport theory aims at deriving this relationship, using elements of the space P as input data. This theory underlies numerous retrieval algorithms (see this issue, for example). Usually, retrieval techniques rely on a model. This provides a direct relationship between measured data and biophysical parameters. It allows for the design of fast retrieval algorithms. However, such algorithms can retrieve only those variables that are explicitly represented in the canopy radiation models. They exclude the use of a rather wide family of three-dimensional models in which desired variables may not be in the model parameter list directly (Ross and Marshak, 1984) (Myneni, 1991) (Borel *et al.*, 1991) (Kimes, 1991) (Knyazikhin *et al.*, 1996). Therefore we cast aside the idea of trying to relate a retrieval technique with a particular canopy radiation model. A method to design simple relationships between the spaces of canopy realization and canopy reflectances allowing the use of three-dimensional models of canopy structure is discussed in section 2.2.

An inverse problem is said to be set up if the spaces P and D, and the function F are specified. The spaces P and D are related as $D=F(P)=\{F(p): p\in P\}$; that is, the space of all possible observations of canopy reflectances consist of the elements $F(p)$ where p runs over the space P. The spaces of canopy realizations and observations of canopy reflectances are static elements of the retrieval algorithm, i.e., the look-up-table. We start a set-up of the inverse problem with the formulation of the following sub-problem: given element $d=(d_{\text{RED}},d_{\text{NIR}})\in D$ find all $p\in P$ for which

$$F(p) = d. \qquad (2.1)$$

Here d_{RED} and d_{NIR} are measured reflectances at red and near infrared wavelengths. This equation allows for multiple solutions. Let $S(d)$ be the set of all solutions of (2.1). The "size" of this set varies with d. The next step is to specify the distribution of a retrieved parameter in the set $S(d)$. Let x be a parameter we retrieve. Leaf area index or FPAR can serve as examples of x. Note that this parameter is not assumed to be included in the vector p characterizing the vegetation canopy. However we assume that it can be evaluated for each given p; that is, the desired parameter is a function of p: $x=\zeta(p)$. For each $d \in D$, a solution distribution function is introduced as follows. One counts numbers $N(d)$ and $N(x,d)$ of different values of $\zeta(p)$ and those of them for which $\zeta(p)$ is less than a given value x. Here p runs over the set $S(d)$. The solution distribution function $\Phi(x,d)$ is defined as the ratio of $N(x,d)$ to $N(d)$; that is, $\Phi(x,d)= N(x,d)/N(d)$. A precise mathematical definition of how to count "continuous" values of $\zeta(p)$ is presented in (Knyazikhin *et al.*, 1998b). The solution distribution function is defined to be the solution of the inverse problem. A desired parameter can now be evaluated as a weighted mean in accordance with the frequency of occurrence of a given value of x, namely,

$$\bar{x}(d) = \int x \, d\Phi(x,d) \,, \qquad (2.2)$$

where the integration is performed over the interval of all possible variations of x. We note some properties of this estimation (Knyazikhin *et al.*, 1998b): Equation (2.1) is sensitive to values of $\zeta(p)$, but not to the canopy realizations p generating the same value of the parameter x. This allows the use of three-dimensional models of canopy structure for which a retrieved parameter may not be in the model parameter list. If the inverse problem has a unique solution for a given d, then (2.2) coincides with this solution.

Figures 5-7 illustrate various aspects of the above definitions for the LAI/FPAR retrieval algorithm. In this case, the inverse problem can be formulated as follows: given canopy reflectances at sensor spectral bands and biome type find all values of ground cover g, mean LAI of an individual plant L and patterns of ground reflectances which satisfy equation (2.1). Here the desired parameter x is LAI. The function $\zeta(p)$ takes the form $\zeta(p)=gL$. The total number of solutions of (2.1) for 40 pixels of different reflectances d are plotted in Figure 5. Figure 6 presents the number of different values of $\zeta(p)$ when p runs over the set $S(d)$. Figure 7 demonstrates the function $\Delta\Phi(\text{LAI}, d)=\Delta\Phi(\text{LAI}+0.25, d) - \Phi(\text{LAI}, d)$ for five different pixels.

The above formulation of the inverse problem presupposes that the spaces P and D and their relationship F are known exactly; that is, $D=D^*$, the space P describes all canopy realizations encountered in reality and F provides correct correspondence between canopy structure and canopy reflectance. In reality however any model can simulate a process only to within a certain degree of accuracy. Also, measurements cannot be carried out exactly. This means that the model predicts a domain O_F around $F(p)$ to which the "true reflectance" belongs. In Figure 1 this domain is schematically shown as a white dot. The same is true for measured reflectances; that is, we can only specify a neighborhood O_d around a measured reflectance d to which the "true value" belongs. Any elements from these domains with high probability can be true values. The neighborhoods O_F and O_d are domains of uncertainties in the measurements and simulations. They depend on the direction Ω_0 of direct solar radiance, view direction Ω and the

ratio f_{dir}. In terms of these notations, we formulate the inverse problem for a single-angle sensor as follows: given measured canopy reflectance d and its domain of uncertainty O_d find all $p \in P$ and their solution distribution function $\Phi_\delta(x,p)$ for which the function F generates canopy reflectances comparable with measured data; that is,

$$F(p) \in O_d. \tag{2.3}$$

The domain O_d can be approximated by an ellipse with the major and minor axes δ_{RED} and δ_{NIR}. The symbol δ denotes the vector $(\delta_{RED},\delta_{NIR})$. In terms of these notations equation (2.3) can be rewritten as:

$$\left(\frac{F_{RED}(p)-d_{RED}}{\delta_{RED}}\right)^2+\left(\frac{F_{NIR}(p)-d_{NIR}}{\delta_{NIR}}\right)^2 \le 1 \quad . \tag{2.4}$$

Values δ_{RED} and δ_{NIR} are uncertainties in measurements and simulations. They depend on the direction Ω_0 of direct solar radiance, view direction Ω and the ratio f_{dir}. Uncertainties are assumed known and serve as input for the retrieval algorithm. Thus (2.3) is reduced to the solution of inequality (2.4). Figures 5-7 illustrate solutions of (2.4) and their distribution function Φ_δ when

$$\delta_{RED} = \delta_{NIR} = \varepsilon(d^2_{RED}+d^2_{NIR})^{1/2}. \tag{2.5}$$

Here ε is the mean uncertainty. The inverse problem for multi-angle sensors can be formulated in a similar way (Knyazikhin *et al.*, 1998b).

The problem is said to be well-posed if the function Φ_δ converges to Φ when δ tends to zero; that is, the more accurate F describes the relationship between canopy realization and their reflectances and the more accurate measured information is, the more accurate the algorithm output would be. If this convergence process does not take place, the problem is defined to be ill-posed.

Inclusion of additional information into retrieval techniques is a basic method to develop algorithms for the solution of ill-posed problems (Tikhonov and Arsenin, 1986). It may be done by limiting the range of variation of the variables determining the three-dimensional radiative regime in plant canopies (quantitative method) and/or by incorporating more equations describing within-canopy radiation regime into retrieval algorithms (qualitative method).

2.2. Optimization of the look-up table: qualitative method

The sets P and D which represent all possible canopy realizations and corresponding observations of canopy reflectances, are static tables in the algorithm, i.e., look-up table. The algorithm interacts only with elements of these sets. This provides independence from a particular canopy radiation model. Theoretically, these sets can be generated offline by solving the transport equation at all instrument spectral bands for various combination of Sun-sensor geometry and all canopy realizations from the set P. However, one can realize it only if the set D can be reprocessed with minimum effort. The time required to precompute this set is a direct function of the number of spectral channels used, combinations of Sun-sensor geometry, and

elements in the set *P*. For example, the generation of the set *D* using this direct method takes approximately 192 computer hours of a medium performance IBM RS/6000 RISC workstation (Running *et al*., 1996). The size of *D* containing canopy reflectances for two spectral bands and for six canopy structural types of global vegetation is about 63 megabites. The inclusion of more spectral bands and view directions leads to significant demands on the core memory required to execute this algorithm. A question then arises as to how the look-up table has to be build. In answering this question, we aimed (1) to minimize the size of the look-up table; (2) to minimize its dependence on a particular canopy radiation model; (3) to make the algorithm as simple as the one linked to a particular canopy radiation model; and (4) to include more qualitative information about the radiative transfer process in order to provide convergence of the algorithm under minimum conceptual limitations. The aim of this section is to discuss some model-independent properties of radiative transfer which help us to meet these requirements.

The monochromatic intensity $I_\lambda(r,\Omega)$ of a three-dimensional radiative field at wavelength λ, at a spatial point r and in direction Ω can be represented as a sum of two components; that is,

$$I_\lambda(r,\Omega) = I_{bs,\lambda}(r,\Omega) + I_{rest,\lambda}(r,\Omega). \tag{3.1}$$

The first component, $I_{bs,\lambda}$, describes the radiative regime within the vegetation canopy for the case of a black surface, and $I_{rest,\lambda}$ describes additional radiative field due to the interaction between the surface and canopy.

This representation takes a simple form when the vegetation canopy can be idealized as a horizontally homogeneous medium bounded at the bottom by a Lambertian surface. The term $I_{rest,\lambda}$ can be expressed as follows (Stamnes, 1982):

$$I_{rest,\lambda} = \frac{\rho_\lambda}{1-\rho_\lambda R_\lambda} T_{bs,\lambda} I_{S,\lambda}. \tag{3.2}$$

Here ρ_λ is albedo of the Lambertian surface, $T_{bs,\lambda}$ is the downward flux at the surface level for the case of the black surface; $I_{S,\lambda}$ and R_λ are radiance and downward flux at the surface level generated by an isotropic wavelength-independent source located at the canopy bottom. Thus one needs three independent variables to describe the radiative regime in the plane-parallel medium. They are reflectance properties of the surface, which do not depend on the vegetation, and $I_{bs,\lambda}$ and $I_{S,\lambda}$, which are surface independent parameters since no multiple interaction of radiation between surface and canopy is possible, i.e., these variables have intrinsic canopy information.

Somewhat more complicated techniques, adjoint formulation and Green's function concept, have been developed in reactor physics to extend the representations (3.1) and (3.2) for the case of three-dimensional radiation field (Bell and Glasstone, 1970). Although in the 3D case $I_{rest,\lambda}$ cannot be expressed in such a simple form, the physical meaning of (3.1) and (3.2) remains unchanged; that is, a three-dimensional radiation field can be parameterized in terms of surface reflectance properties which are independent on vegetation; the radiation field in the vegetation canopy for the case of the black surface ("Black soil problem"); and the radiation field in the vegetation canopy generated by anisotropic heterogeneous wavelength-independent sources located at the canopy bottom ("S problem"). Recently this technique was used to create the look-up table for the MODIS and MISR LAI/FPAR retrieval algorithm (Knyazikhin *et al*., 1998a). In

terms of this approach the hemispherical directional reflectance factor (HDRF) d_λ at wavelength λ can be expressed as:

$$d_\lambda(\Omega,\Omega_0) \approx \pi w_{\mathrm{bs},\lambda}\mathbf{r}_{\mathrm{bs},\lambda}(\Omega_0) + \pi w_{\mathrm{S},\lambda}\mathbf{t}_{\mathrm{S},\lambda}\frac{\rho_{\mathrm{eff}}(\lambda)}{1-\rho_{\mathrm{eff}}(\lambda)\mathbf{r}_{\mathrm{S},\lambda}}\mathbf{t}_{\mathrm{bs},\lambda}(\Omega_0). \quad (3.3)$$

Here $\mathbf{r}_{\mathrm{bs},\lambda}$ and $\mathbf{r}_{\mathrm{S},\lambda}$ are hemispherically integrated canopy reflectances (bihemispherical reflectance, BHR), and $\mathbf{t}_{\mathrm{bs},\lambda}$ and $\mathbf{t}_{\mathrm{S},\lambda}$ are canopy transmittance for the "black soil problem" and "S problem," respectively; the weight $w_{\mathrm{bs},\lambda}$ is the ratio of the HDRF for the "black soil problem" to $\mathbf{r}_{\mathrm{bs},\lambda}$; and $w_{\mathrm{S},\lambda}$ is the ratio of the canopy leaving radiance generated by anisotropic sources on the canopy bottom to $\mathbf{t}_{\mathrm{S},\lambda}$. The effective ground reflectance ρ_{eff} is the fraction of radiation reflected by the canopy ground. This variable depends on the "complete" radiation regime in the vegetation canopy. However its range of variations does not exceed the range of variations of the hemispherically integrated bidirectional factor of the ground surface which is independent on the vegetation (Knyazikhin *et al.*, 1998a). Therefore ρ_{eff} can be taken as a parameter characterizing the ground reflection. The set of various patterns of spectral effective ground reflectances is a static table of the retrieval algorithm. The radiation reflected ($\mathbf{r}_{\mathrm{bs},\lambda}$ and $\mathbf{r}_{\mathrm{S},\lambda}$), transmitted ($\mathbf{t}_{\mathrm{bs},\lambda}$ and $\mathbf{t}_{\mathrm{S},\lambda}$) and absorbed ($\mathbf{a}_{\mathrm{bs},\lambda}$ and $\mathbf{a}_{\mathrm{S},\lambda}$) by the vegetation are related via the law of energy conservation as:

$$\mathbf{r}_{\mathrm{bs},\lambda} + \mathbf{t}_{\mathrm{bs},\lambda} + \mathbf{a}_{\mathrm{bs},\lambda} = 1, \quad (3.4)$$

$$\mathbf{r}_{\mathrm{S},\lambda} + \mathbf{t}_{\mathrm{S},\lambda} + \mathbf{a}_{\mathrm{S},\lambda} = 1, \quad (3.5)$$

Thus the canopy reflectance is parameterized in terms of the effective ground reflectance, and solutions of the "black-soil problem" and the "*S* problem." The solution of the "black-soil problem" depends on Sun-view geometry, canopy architecture, and spectral properties of the leaves. The solution of the "*S* problem" depends on the spectral properties of the leaves and canopy structure only. These properties allow a significant reduction in the size of the LUT because there is no need to store the dependence of the exiting radiation on ground reflection properties. Elements of *D* can be composed from precomputed solutions of the "black-soil problem" and "*S* problem" and precomputed values of the effective ground reflectance. Note that the BHRs $\mathbf{r}_{\mathrm{bs},\lambda}$ and $\mathbf{r}_{\mathrm{S},\lambda}$ are not included in the LUT. Given canopy absorptance and transmittance they are evaluated via the energy conservation law (3.4) and (3.5). This makes the canopy reflectance sensitive to the within-canopy radiation regime ($\mathbf{t}_{\mathrm{bs},\lambda}$, $\mathbf{a}_{\mathrm{bs},\lambda}$, $\mathbf{t}_{\mathrm{S},\lambda}$, $\mathbf{a}_{\mathrm{S},\lambda}$). This approach is an example of the inclusion of qualitative information into the retrieval algorithm.

Assuming validity of the energy conservation law for any canopy elementary volume, the following simple dependence of canopy absorptance for the "black soil problem" (subscript κ="bs") and "S problem" (κ="S") on wavelength can be precisely derived (Knyazikhin *et al.*, 1998a):

$$\mathbf{a}_{\kappa,\lambda} = \frac{1-\omega(\lambda_0)p_\kappa}{1-\omega(\lambda)p_\kappa}\frac{1-\omega(\lambda)}{1-\omega(\lambda_0)}\mathbf{a}_{\kappa,\lambda_0}. \quad (3.6)$$

Here $\omega(\lambda)$ is the leaf albedo; p_κ is a wavelength independent coefficient defined as

$$p_\kappa = \frac{\int_V \int_{4\pi} I_{\kappa,\mathrm{b}}(r,\Omega)\sigma(r,\Omega)\,dr d\Omega}{\int_V \int_{4\pi} I_{\kappa,\mathrm{w}}(r,\Omega)\sigma(r,\Omega)\,dr d\Omega}, \qquad (3.7)$$

where $I_{\kappa,\mathrm{b}}$ and $I_{\kappa,\mathrm{w}}$ are solutions of the "Black soil problem" (κ="bs") and "S problem" (κ="S") for "black" (ω=0) and "white" (ω=1) leaves; and σ is the total interaction cross-section (which does not depends on wavelength). Similar relationships can also be derived for canopy transmittance (Knyazikhin *et al*., 1998a).

Note that $\omega(\lambda)p_\kappa$ is the critical eigenvalue of the transport equation. This eigenvalue plays an important role in transport theory, for instance, in neutron transport theory. It alone determines if the fissile assembly will function as a reactor, or as an explosive, or will melt. Its value successfully relates the reactor geometry to the absorption capacity of the active zone. Because the reactor is controlled by changing the absorption capacity of the active zone (by inserting or removing absorbents), this value is critical to its functioning. The similarity to the problem at hand is that we need to relate canopy architecture ("similar" to reactor geometry) with leaf optical properties ("similar" to the absorption capacity of the active zone). Therefore we apply this technique to derive relationships between spectral leaf albedo, canopy structure (coefficient p_κ) and canopy absorptance and transmittance.

Thus given canopy absorptance and transmittance for "Black soil" and "S problem" at a reference wavelength λ_0, one can evaluate these variables at any other wavelength λ. Therefore there is no need to store the wavelength dependencies in the look-up table, i.e., information on canopy structure is stored in the look-up table only. Integrated canopy reflectances can then be evaluated via the energy conservation law (3.4) and (3.5). This facilitates comparison of spectral values of the canopy reflectances with spectral properties of individual leaves, which is a rather stable characteristic of a green leaf. It also can be interpreted as "inclusion of additional qualitative information" into the algorithm, thus allowing a significant reduction in the number of retrieved solutions (i.e., the size of the set $S(d)$).

2.3. Conservativity as a tool to constrain retrieval

A radiative transfer model is defined to be conservative if the law of energy conservation holds true for any elementary volume [*Bass et al*., 1986]. Within a conservative model, radiation absorbed, transmitted, and reflected by the canopy is always equal to radiation incident on the canopy. However a rather wide family of canopy radiation models designed to account for the hot spot effect (Kuusk, 1985) (Marshak, 1989) (Pinty *et al*., 1989) (Li and Strahler, 1992) (Myneni *et al*., 1995) conflict with the law of energy conservation (Knyazikhin *et al*., 1998a). These types of canopy radiation models are mainly used to fit simulated HDRFs to measured HDRFs. However, the ability of a model to simulate canopy reflection is not a sufficient requisite for the solution of the ill-posed problem. Canopy radiation models must also satisfy the law of energy conservation and provide the correct proportions of canopy absorptance, transmittance, and reflectance.

In spite of the diversity of canopy reflectance models, their direct use in an inversion algorithm may be ineffective. In the case of forests, for example, the interaction of photons with

the rough and rather thin surface of tree crowns and with the ground in between the crowns are the most important factors causing the observed variation in the directional reflectance distribution. These phenomena are rarely captured by many canopy reflectance models. As a result, these models are only slightly sensitive to the within-canopy radiation regime. On the other hand, it is the within-canopy radiation regime that is sensitive to the canopy structure. The within-canopy radiation regime also determines the amount of solar energy absorbed by the vegetation. Ignoring this phenomenology in canopy radiation models leads to a large number of nonphysical solutions when one directly inverts a canopy reflectance model.

Results presented in section 2.2 are valid for conservative models only. This sets requirements of the canopy reflectance models used to generate the look-up table. Equations (3.3)-(3.5) allow the formulation of a test for the "eligibility" of a canopy radiation model to generate the look-up table. First the weight $w_{bs,\lambda}$ is evaluated as a function of Sun-view geometry, wavelength, and LAI by using a field-tested canopy reflectance model. Then, with the same model, $\mathbf{r}_{bs,\lambda}$ and $\mathbf{r}_{S,\lambda}$ are evaluated from (3.4) and (3.5) and inserted into (3.3). A canopy radiation model is "eligible" to generate the look-up table if (3.3) is satisfied to within a given accuracy for any combination of Sun-view geometry, wavelength, LAI and effective ground reflectance. We do not know of a canopy reflectance model which can pass this test. It is because there is no published model thus far which satisfies the energy conservation law. The success of development of canopy radiation models and their applications depends, to a high degree, upon being able to derive a canopy transport equation which, from the one hand, allows for the hot spot effect, and, from the other hand, is conservative.

2.4. Examples of global LAI and FPAR fields derived by using look-up table approach

The look-up table approach was implemented into the standard processing algorithm for producing global LAI and FPAR fields from canopy reflectance data measured by MODIS and MISR instruments aboard the EOS-AM 1 platform. This algorithm was prototyped with atmospherically corrected SeaWiFs, LASUR, LANDSET and POLDER data. Here some results on prototyping the LAI/FPAR algorithm with SeaWiFS and LASUR data sets are presented.

Data used

SeaWiFS (Sea-viewing Wide Field-of-view Sensor) data set includes global daily atmospherically corrected surface reflectances at 412, 443, 490, 510, 555, 670, 765, 865 nanometers. We used surface reflectances at 443, 555, 670 and 865 nm at 8 kilometer resolution for the period 18 Sep – 12 Oct 1997.

LASUR (LAnd SUrface Reflectances) is a data set of atmospherically corrected surface reflectances in the red (572-698 nm) and Near-InfraRed (NIR, 716-985 nm) channels of the Advanced Very High Resolution Radiometer (AVHRR) at global scale (1/7,1, and 5 square degree resolution; one week temporal resolution) for 1989 and 1990.

BCM (Biome Classification Map) contains the distribution of six canopy structural types (biomes). This data set was derived from AVHRR Pathfinder data set (Myneni *et al.*, 1997] and, thus, is independent on the SeaWiFS data used. Contrary to the SeaWiFS data, the BCM is the static file, i.e., it is a time-independent data set. This data set was taken as a prototype of the MODIS Land Cover Product which is required by the MODIS LAI/FPAR algorithm.

Uncertainties

Both atmospherically corrected BRF's (Bi-directional Reflectance Factor) and their uncertainties δ (see section 2.1) are inputs to the algorithm. However, the SeaWiFS data set has no information on the uncertainties in BRF's. Therefore, we used (2.5) to describe this input variable. The same formula is used by the MODIS LAI/FPAR algorithm (version 2.1). A special technique was developed by the MISR team to evaluate uncertainties in retrieved canopy reflectances (Martonchik *et al.*, 1998). Therefore, both atmospherically corrected canopy reflectances and their uncertainties are inputs for the MISR version of the algorithm. In our prototyping activities, the mean uncertainty ε was supposed constant. In the results presented here, its value was 0.2, which was derived by analyzing the retrieved LAI and FPAR values (see sub-section “Success index”).

Execution of the algorithm

The LAI/FPAR algorithm was run for each pixel using SeaWiFS, LASUR and BCM data sets. Results presented here are referred to pixels classified by the BCM as biome 1 (Grasses and Cereal Crops) and to July 10-17, 1990 (LASUR) and September 22, 1997 (SeaWiFS). The algorithm was executed for every pixel, whether it was vegetated or not.

Success index

It may be the case that equation (2.4) has no solutions. The following characteristics of the table look-up method are introduced. A pixel for which the algorithm retrieves a value of LAI and FPAR is termed a successful pixel. A pixel for which equation (2.4) has no solutions is termed an unsuccessful pixel. The ratio of the number of successful pixels to the total number of pixels is the success index.

Figure 8 demonstrates the dependence of the success index on the mean uncertainty ε. The success index increases with the increase of ε. However the quality of LAI/FPAR product decreases with the increase of the mean uncertainty. If ε is underestimated, the algorithm fails when real uncertainties in surface reflectances are greater than one determined by (2.5). If, however, the mean uncertainty is overestimated, the algorithm can produce LAI/FPAR values for non-vegetated pixels. Therefore, there should be a critical value of ε for which equation (2.5) optimally approximates real uncertainties. A solution of the following problem was taken as the critical value: find such ε for which 95% of unsuccessful pixels are non-vegetated. Solutions to this problem were 0.15 for the LASUR, and 0.20 for the SeaWiFS data.

Distribution of unsuccessful pixels

Figure 9 demonstrates the distribution of pixels from SeaWiFS data set (Grasses and Cereal Crops) with respect to their reflectances at near-infrared and red wavelengths. The left panel shows successful, and the right panel unsuccessful pixels. The success index is 0.73. Figure 10 shows the distribution of unsuccessful pixels with respect to the NDVI values. One can see that 81% of unsuccessful pixels have a negative value of NDVI. The second class of unsuccessful pixels (16%) is one where NDVI values were between 0 and 0.1. Thus, 97% of unsuccessful pixels can not be considered as vegetated pixels. This example demonstrates that equation (2.4)

has no solutions when the pixels are non-vegetated or data are corrupted due clouds or atmosphere effect provided the mean uncertainty is chosen correctly.

Test of physics

Figure 11 demonstrates the distributions of retrieved values of LAI and FPAR with respect to the SeaWiFS and LASUR NDVI fields. Two bands, 670 and 865 nm, from the SeaWiFS data set were used to evaluate LAI and FPAR. The LAI-NDVI and FPAR-NDVI relationships derived from the algorithm correspond to those reported in literature. This example indicates that the solution distribution function which is taken as the solution of the inverse problem provides correct statistical properties of retrieval parameters.

Using various combinations of the instrument spectral bands in the retrieval

Table 1 summarizes the use of different combinations of spectral bands in the retrieval algorithm. If NDVI was less than 0.1, the pixel was considered to be non-vegetated, and the algorithm was not executed in tests presented in this sub-section. Therefore, the success index was calculated as the ratio of the number of successful pixels to the total number of pixels for which NDVI>0.1.

The use of the blue band results in poor retrievals. The following arguments can be presented. The optical properties of foliage elements at blue and red wavelengths are similar. Thus the surface reflectances are comparable in magnitude. However atmospheric effect at blue band is much stronger than at the red band. As a result, the uncertainties in the atmospherically corrected BRF's data are greater at blue than at red band. In prototyping the algorithm we assumed that uncertainties in LASUR and SeAWiFS data sets were wavelength independent. Thus the algorithm processes the blue and red BRF's with equal weight. The use of blue BRF therefore results in poorer retrievals. Holding the mean uncertainty ε constant, all combinations of spectral bands without the blue provide better results than ones including the blue band. Evaluation of the uncertainties in atmospherically corrected surface reflectances (Martonchick *et al*., 1998) is critical to improve the quality of the LAI/FPAR product, and to realize the full potential of the modern satellite-born sensors.

Prototype of the MODIS LAI/FPAR data standard product

SeaWiFS data. The algorithm was applied to daily surface reflectance data at the 8 km resolution for all days from 18 Sep to 12 Oct 1997. For each pixel, LAI and FPAR values corresponding to the maximum NDVI during this period are shown in Plate 1.

LASUR data. The above algorithm was applied to the weekly surface reflectance data (8 km) for 4 weeks in January and for 4 weeks in July. Plate 2 shows the color-coded images of global LAI in January and in July composited based on maximum NDVI during those four weeks. The global FPAR images in the same months are presented in Plate 3.

2.5. Research issues

- Retrieval of vegetation parameters as ill-posed problem.

- Distribution of multiple acceptable parameters as the solution of inverse problems.
- Uncertainties in measurements and simulations as input to retrieval algorithms.
- Three-dimensional canopy structure models as a basis of retrieval algorithms.
- Development of conservative canopy radiation models as a key issue to improve the retrieval capacity of inversion techniques, and to realize the full potential of the modern satellite-born sensors.

References

Bass, L.P., A.M.Volocsvhenko, and T.A.Germogenova (1986) *Methods of Discrete Ordinates in Radiation Transport Problems*. Moscow: Inst. Appl. Math., Russ. Acad. of Sci., 231 pp. (in Russian, with English abstract).

Bell, G. I., and S. Glasstone (1970) *Nuclear Reactor Theory*. New York: Van Nostrand Reinholt, 619 pp.

Borel, C.C., S.A., Gerstl, and B.J. Powers (1991) The radiosity method in optical remote sensing of structured 3-D surfaces. *Remote Sens. Environ.*, **36:** 13-44.

Borel-Donohue, C. C. (1988) Models for back scattering of millimeter waves from vegetative canopies. PhD Thesis, Dept. Electrical and Computer Eng., Univ. of Massachusetts at Amherst, Mass 01003.

Chen, S. G., B.Y. Shao, I. Impens, and R. Ceulemans (1994) Effect of plant canopy structure on light interception and photosynthesis, *J. Quant. Spectrosc. Radiat. Transfer*, **52:** 115-123.

de Reffye, P., P. Dinouard, and D. Barthélémy (1991) Modélisation et simulation de l'architecture de l'orme du japon Zelkova Serrata (Thunb.) Makino (Ulmaceae): La notion d'axe de référence. In *Naturalia Monspeliensia*, Montpellier, France, 251-266.

Diner, D.J., J.V.Martonchik, C. Borel, S.A.W. Gerstl, H.R. Gordon, Y. Knyazikhin, R. Myneni, B. Pinty, and M.M. Verstraete (1998) MISR: Level 2 surface retrieval algorithm theoretical basis. *JPL Internal Doc. D-11401, Rev. C*, Calif. Inst. of Technol., Jet Propul. Lab., Pasadena, 96 p.

Kimes, D.S. (1991) Radiative transfer in homogeneous and heterogeneous vegetation canopies. In: *Photon-Vegetation Interactions: Applications in Plant Physiology and Optical Remote Sensing* (R. B. Myneni and J. Ross eds.). New York: Springer-Verlag, pp. 339-388.

Kimes, D.S., P,J. Sellers, and D.J. Dinner (1987) Extraction of spectral hemispherical reflectance (albedo) of surfaces from nadir and directional reflectance data. *Int. J. Rem. Sens*., **8**, 1727.

Knyazikhin, Y., J.V. Martonchik, D.J.Diner, R.B. Myneni, M.M. Verstraete, B.Pinty, and N. Gobron (1998b) Estimation of vegetation canopy leaf area index and fraction of absorbed photosynthetically active radiation from atmosphere-corrected MISR data. *J. Geophys. Res.* (in press).

Knyazikhin, Y., J.V., Martonchik, R.B. Myneni, D.J. Diner, and S.W. Running (1998a) Synergistic algorithm for estimating vegetation canopy leaf area index and fraction of absorbed photosynthetically active radiation from MODIS and MISR data. *J. Geophys. Res*. (in press).

Knyazikhin, Yu., Kranigk, J., Miessen, G., Panfyorov, O, Vygodskaya, N. and Gravenhorst, G. (1996) Modelling three-dimensional distribution of photosynthetically active radiation in Sloping coniferous stands. *Biomass and Bioenergy*, **2/3:** 189-200.

Kranigk, J., and G. Gravenhorst (1993) Ein dreidimensionales Modell für Fichtenkronen. *Allg. Forst Jagdztg.*, **164,(8):** 146-149.

Kranigk, J., F. Gruber, J. Heimann, and A. Thorwest (1994) Ein Model für die Kronenraumstruktur und die räumliche Verteilung der Nadeloberfläche in einem Fichtenbestand. *Allg. Forst Jagdztg.*, **165 (10-11)**: 193-197, 1994.

Kurth, W. (1994) Morphological models of plant growth: Possibilities and ecological relevance. *Ecol. Modell.*, **75/76**: 299-308.

Kuusk, A. (1985) The hot spot effect of a uniform vegetative cover. *Sov. J. Remote. Sens.*, **3:** 645-658.

Li, X., and A.H. Strahler (1992) Geometrical-optical bidirectional reflectance modeling of the discrete crown vegetation canopy: Effect of crown shape and mutual shadowing. *IEEE Trans. Geosci. Remote Sens.*, **30:** 276-292.

Marshak, A. (1989) Effect of the hot spot on the transport equation in plant canopies. *J. Quant. Spectrosc. Radiat. Transfer*, **42:** 615-630.

Martonchik, J.V., D.J. Diner, B. Pinty, M.M. Verstraete, R.B. Myneni, Y. Knyazikhin, and H.R. Gordon (1998) Determination of land and ocean reflective, radiative and biophysical properties using multi-angle imaging. *IEEE Trans. Geosci. Remote Sens.*, **36:** 1266-1281.

Myneni, R.B. (1991) Modeling radiative transfer and photosynthesis in three-dimensional vegetation canopies. *Agric. For. Meteorol.*, **55:** 323-344.

Myneni, R.B., R.R. Nemani, and S.W. Running (1997) Estimation of global leaf area index and absorbed PAR using radiative transfer model. *IEEE Trans. Geosci. Remote Sens.*, **35:** 1380-1393.

Pinty, B., M.M.Verstraete, and R.E.Dickenson (1989) A physical model for predicting bidirectional reflectance over bare soils. *Remote Sens. Environ.*, **27:** 273-288.

Ross, J.K., and A. L. Marshak (1984) Calculation of the solar radiation reflection from plant cover using the Monte-Carlo method. *Sov. J. Remote. Sens.*, **5:** 58-67.

Running, S.W., R.B. Myneni, R. Nemani, and J. Glassy. (1996) MOD15 LAI/FPAR algorithm theoretical basis document, MODIS LAI (leaf area index) and MODIS FPAR (fraction of absorbed photosynthetically active radiation). *Tech. Rep.*, Sch. of For., Univ. of Mont., Missoula.

Sellers, P.J. (1985) Canopy reflectance, photosynthesis and transpiration. *Int. J. Rem. Sens.*, **8**: 1335.

Sellers, P.J. (1987) Canopy reflectance, photosynthesis and transpiration II: The role of biophysics in the linearity of their interdependence. *Remote Sens. Env.*, **21**: 143.

Sundquist, E.T. (1993) The global carbon dioxide budget. *Science*, **259**: 934-941.

Tikhonov, A.N., and V. Y. Arsenin (1986) *Methods for Solving Ill-Posed Problems*. Moscow: Nauka, 288 pp. (in Russian)

Figure captions

FIGURE 1. Distribution of vegetated pixels with respect to their reflectances at near-infrared (865 nm) and red (670 nm) wavelengths derived from the SeaFIWS (Sea-viewing Wide Field-of-view Sensor) data set (September 22, 1997). This data set includes global daily atmosphere-corrected surface reflectances at 412, 443, 490,510, 555, 670, 765 and 865 manometers. Each point on the RED-NIR plane can be treated as a vector.

FIGURE 2. Patterns of the architecture on individual trees. (From Kranigk *et al*., 1994)

FIGURE 3 Given architectural patterns of individual trees (Figure 2) and their distribution (left) one can generate the architecture of the entire canopy (right). (From Kranigk *et al*., 1994)

FIGURE 4. Schematic representation of patterns of leaf (left, leaf albedo) and soil (right, soil reflectance) optical spectra.

FIGURE 5. The total number of solutions of (2.4) for 40 pixels of different reflectances. The mean uncertainty ε was 0.2.

FIGURE 6. Number of different solutions of equation (2.4) for 40 pixels of different reflectances. The mean uncertainty ε was 0.2.

FIGURE 7. Localization of probable values of LAI. The function $\Delta\Phi(L,d)=\Phi(L+0.25,d)- \Phi(L,d)$ shows the probability distribution of multiple acceptable solutions for five different pixels. Values of LAI were as follows: Pixel #1: 0.1; pixel #5: 1; pixel #9: 2; pixel #13: 3; pixel #21: 5. The mean uncertainty ε was 0.2.

FIGURE 8. Dependence of the success index on the mean uncertainty ε. The optimum values of ε are 0.20 for the SeaWiFS and 0.15 for LASUR data.

FIGURE 9. Distribution of pixels with respect to their reflectances at near-infrared and red wavelengths derived from the SeaFIWS data set (September 22, 1997). The left plot shows all pixel for which the algorithm was successful. The right plot shows those pixels for which equation (2.4) has no solutions. The algorithm was applied to every pixel marked in the BCM data set as Biome 1 (Grasses and Cereal Crops). The number of successful pixels was 73%; the mean uncertainty was 0.2 in this example.

FIGURE 10. Distribution of "unsuccessful" pixels with respect to NDVI values. One can see that unsuccessful pixels are mainly those for which the NDVI is less than 0.1; that is, non-vegetated pixels.

PLATE 1. (a) Global LAI and (b) FPAR in September-October 1997 derived from SeaWiFs (Sea-viewing Wide Field-of-view Sensor) data. This data set includes daily atmosphere corrected surface reflectances at eight shortwave spectral bands. Surface reflectances at red (670 nm) and near-infrared (865 nm) at 8 kilometer resolution were used. The algorithm was applied to daily surface reflectance data for all days from September 18 to October 12 1997. For each pixel, LAI and FPAR values corresponding to the maximum NDVI during this period are shown in these panels.

PLATE 2. Global LAI derived from LASUR (LAnd SUrface Reflectance) data. This data set includes atmospherically corrected surface reflectances in the red and near-infrared channels of the Advanced Very High Resolution Radiometer (AVHRR) at global scale (1/7,1, and 5 square degree resolution; one week temporal resolution) for 1989 and 1990. The algorithm was applied to the weekly surface reflectance data (8 km) for 4 weeks in January and for 4 weeks in July. These panels show the color-coded images of global LAI (a) in January and (b) in July composited based on maximum NDVI during those four weeks.

PLATE 3. Global FPAR derived from LASUR data. The algorithm was applied to the weekly surface reflectance data (8 km) for 4 weeks in January and for 4 weeks in July. These panels show the color-coded images of global FPAR in January (a) and in July (b) composited based on maximum NDVI during those four weeks.

Table 1
The success index* for various combinations of spectral bands used to retrieve LAI and FPAR.

Spectral bands used				Success index, %
NIR	Red	Blue	Green	
x	x			96.8
x	x		x	95.0
	x		x	94.9
x			x	94.8
x		x		86.5
x		x	x	77.8
x	x	x	x	77.8
x	x	x		75.2

*The success index was calculated here as the ratio of number of successful pixels to the total number of pixels for which NDVI>0.1. Values of the index are expressed in %.

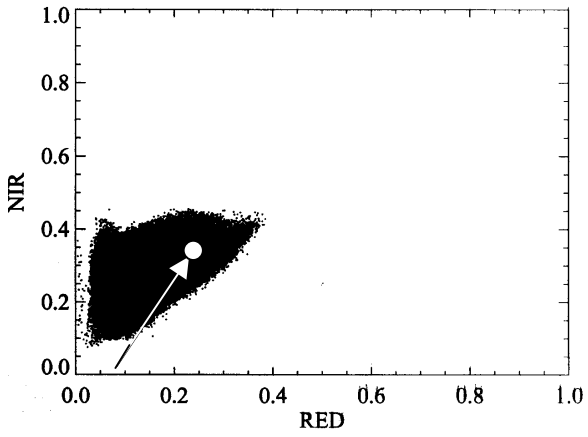

FIGURE 1. Distribution of vegetated pixels with respect to their reflectances at near-infrared (865 nm) and red (670 nm) wavelengths derived from the SeaFIWS (Sea-viewing Wide Field-of-view Sensor) data set (September 22, 1997). This data set includes global daily atmosphere-corrected surface reflectances at 412, 443, 490,510, 555, 670, 765 and 865 manometers. Each point on the RED-NIR plane can be treated as a vector.

FIGURE 2. Patterns of the architecture on individual trees. (From Kranigk *et al.*, 1994)

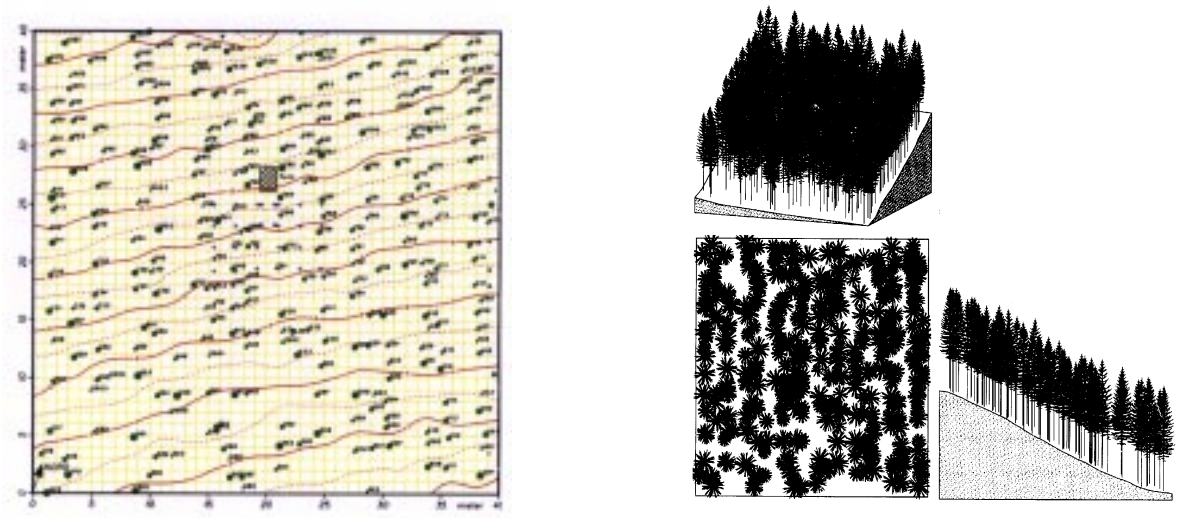

FIGURE 3 Given architectural patterns of individual trees (Figure 2) and their distribution (left) one can generate the architecture of the entire canopy (right). (From Kranigk *et al*., 1994)

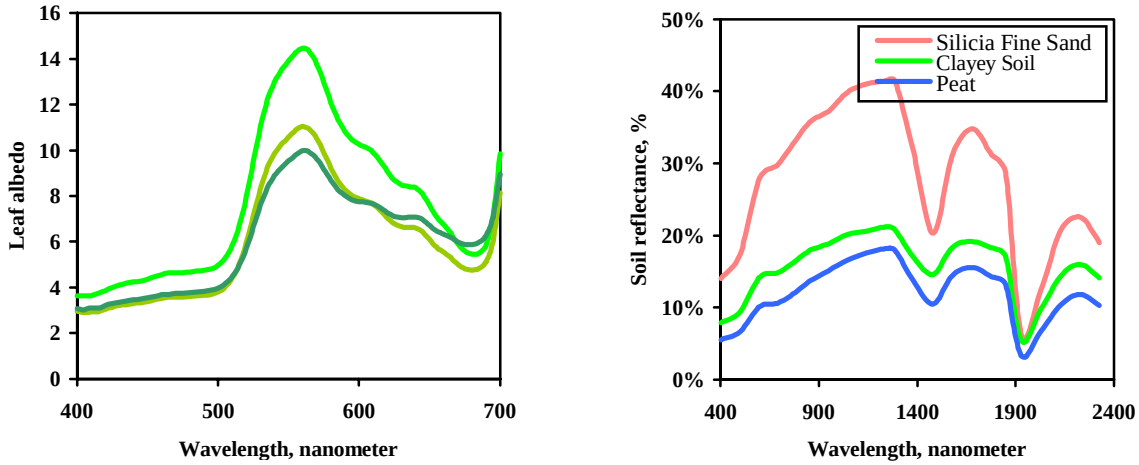

FIGURE 4. Schematic representation of patterns of leaf (left, leaf albedo) and soil (right, soil reflectance) optical spectra.

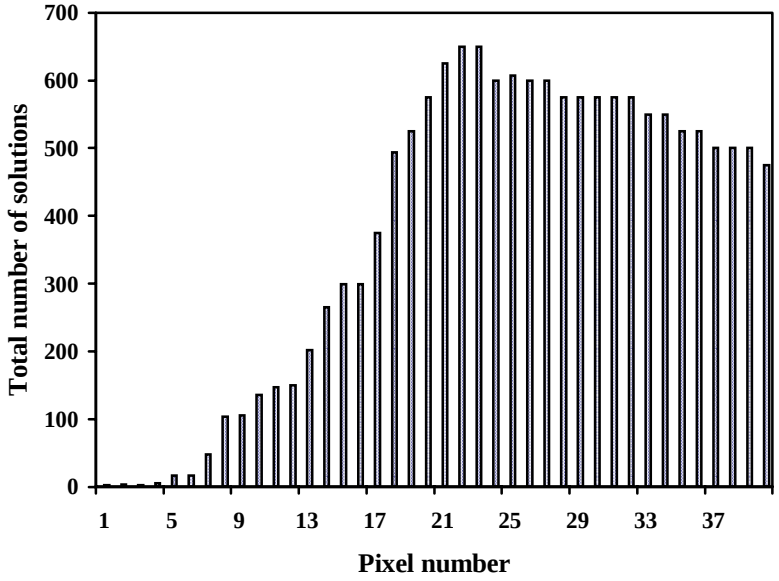

FIGURE 5. The total number of solutions of (2.4) for 40 pixels of different reflectances. The mean uncertainty ε was 0.2.

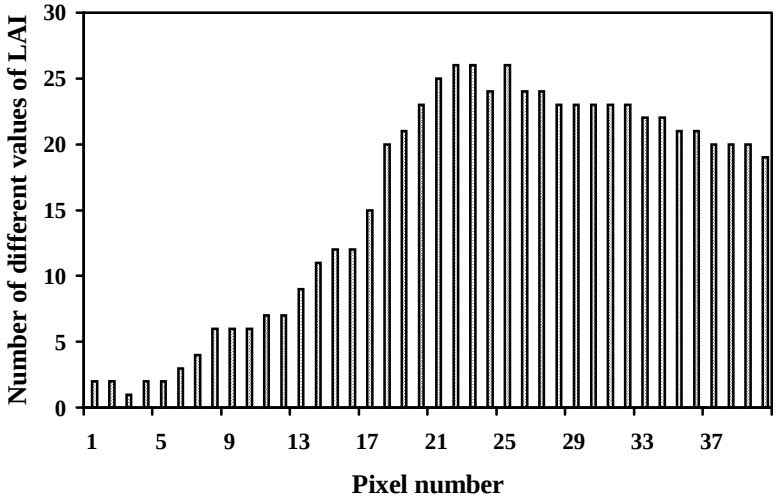

FIGURE 6. Number of different solutions of equation (2.4) for 40 pixels of different reflectances. The mean uncertainty ε was 0.2.

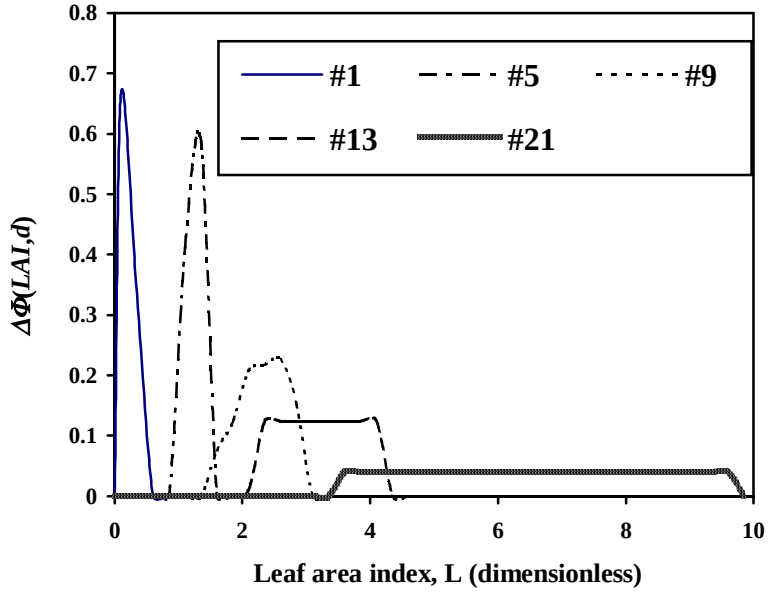

FIGURE 7. Localization of probable values of LAI. The function $\Delta\Phi(L,d)=\Phi(L+0.25,d)-\Phi(L,d)$ shows the probability distribution of multiple acceptable solutions for five different pixels. Values of LAI were as follows: Pixel #1: 0.1; pixel #5: 1; pixel #9: 2; pixel #13: 3; pixel #21: 5. The mean uncertainty ε was 0.2.

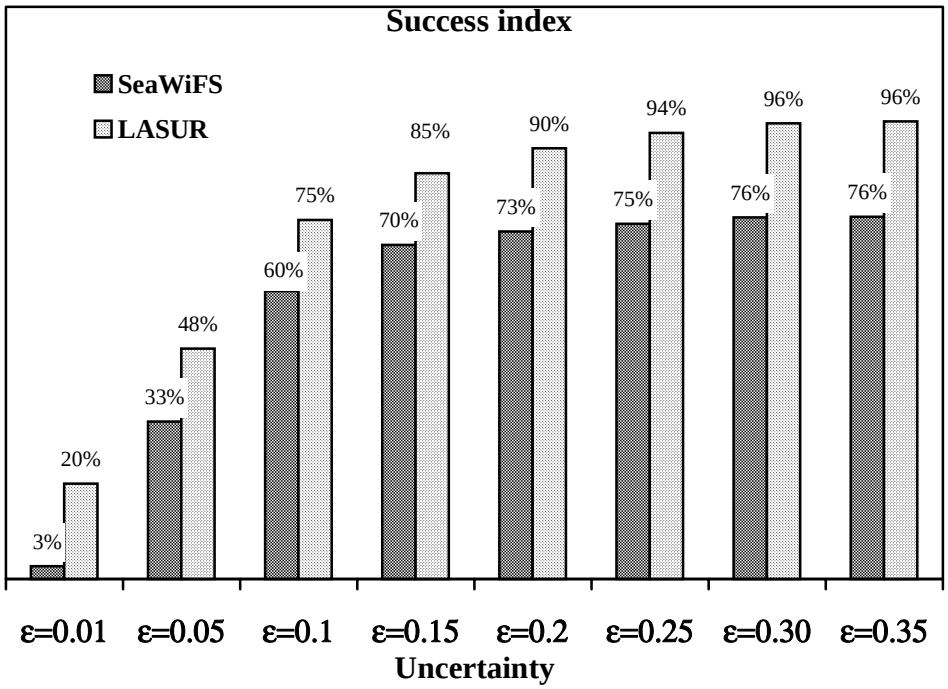

FIGURE 8. Dependence of the success index on the mean uncertainty ε. The optimum values of ε are 0.20 for the SeaWiFS and 0.15 for LASUR data.

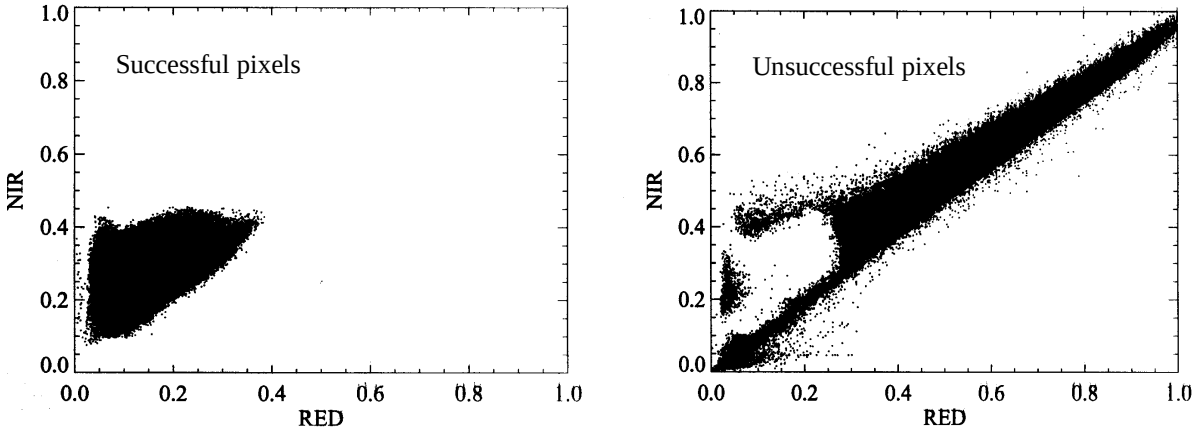

FIGURE 9. Distribution of pixels with respect to their reflectances at near-infrared and red wavelengths derived from the SeaFIWS data set (September 22, 1997). The left plot shows all pixel for which the algorithm was successful. The right plot shows those pixels for which equation (2.4) has no solutions. The algorithm was applied to every pixel marked in the BCM data set as Biome 1 (Grasses and Cereal Crops). The number of successful pixels was 73%; the mean uncertainty was 0.2 in this example.

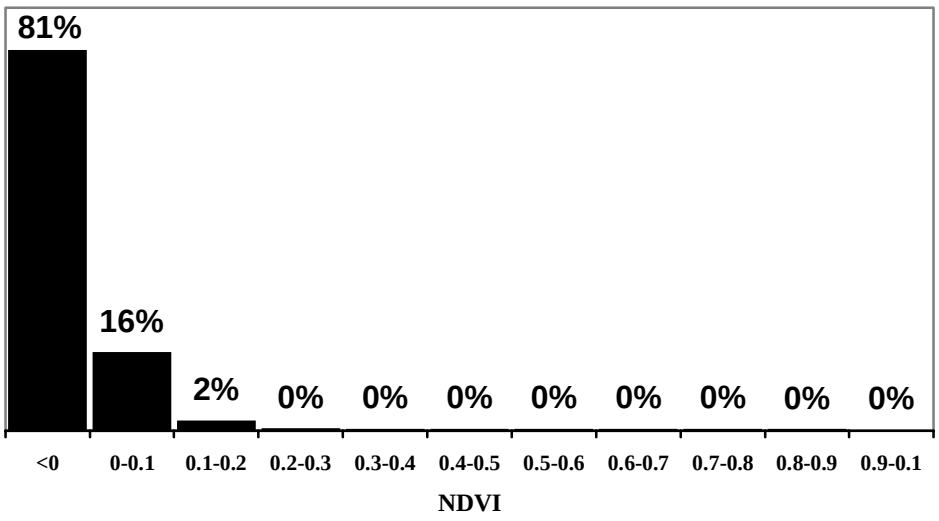

FIGURE 10. Distribution of "unsuccessful" pixels with respect to NDVI values. One can see that unsuccessful pixels are mainly those for which the NDVI is less than 0.1; that is, non-vegetated pixels.

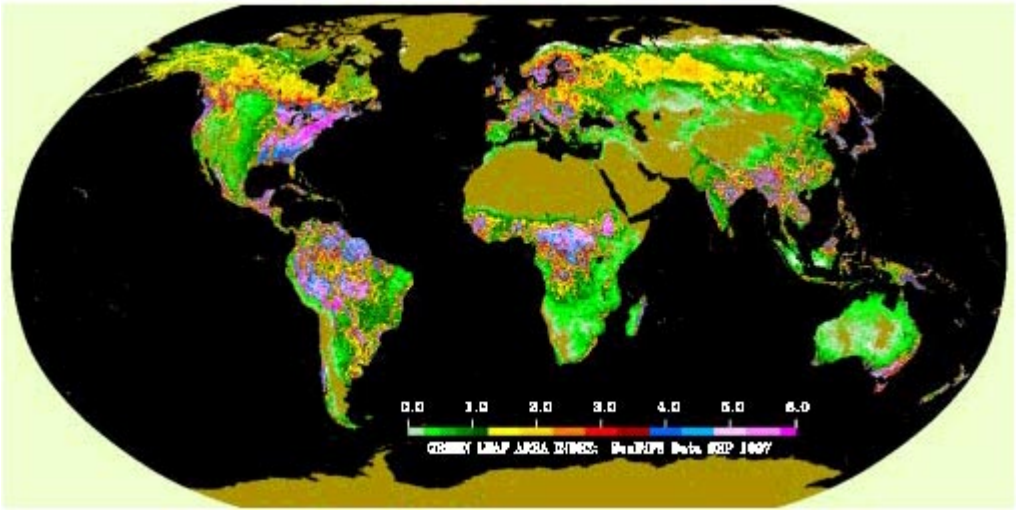

a)

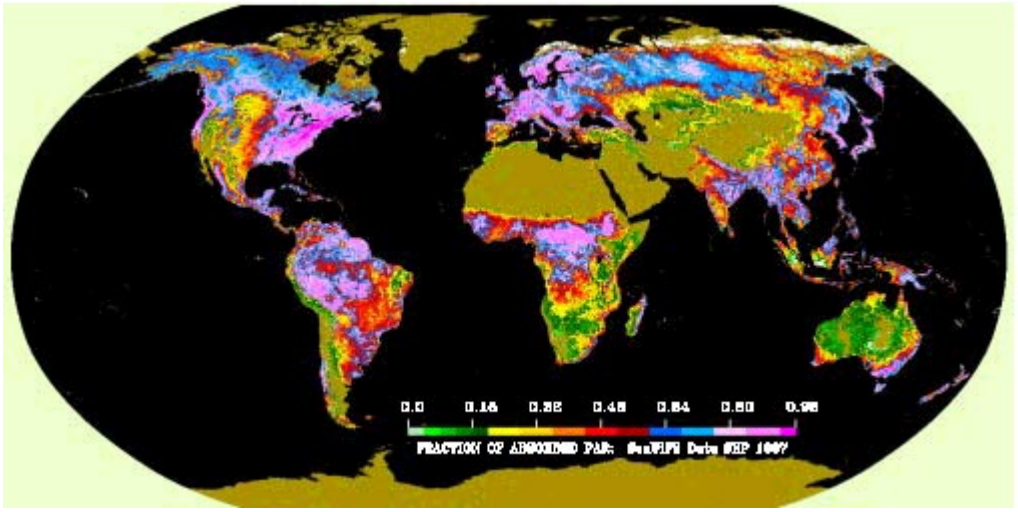

b)

PLATE 1. (a) Global LAI and (b) FPAR in September-October 1997 derived from SeaWiFs (Sea-viewing Wide Field-of-view Sensor) data. This data set includes daily atmosphere corrected surface reflectances at eight shortwave spectral bands. Surface reflectances at red (670 nm) and near-infrared (865 nm) at 8 kilometer resolution were used. The algorithm was applied to daily surface reflectance data for all days from September 18 to October 12 1997. For each pixel, LAI and FPAR values corresponding to the maximum NDVI during this period are shown in these panels.

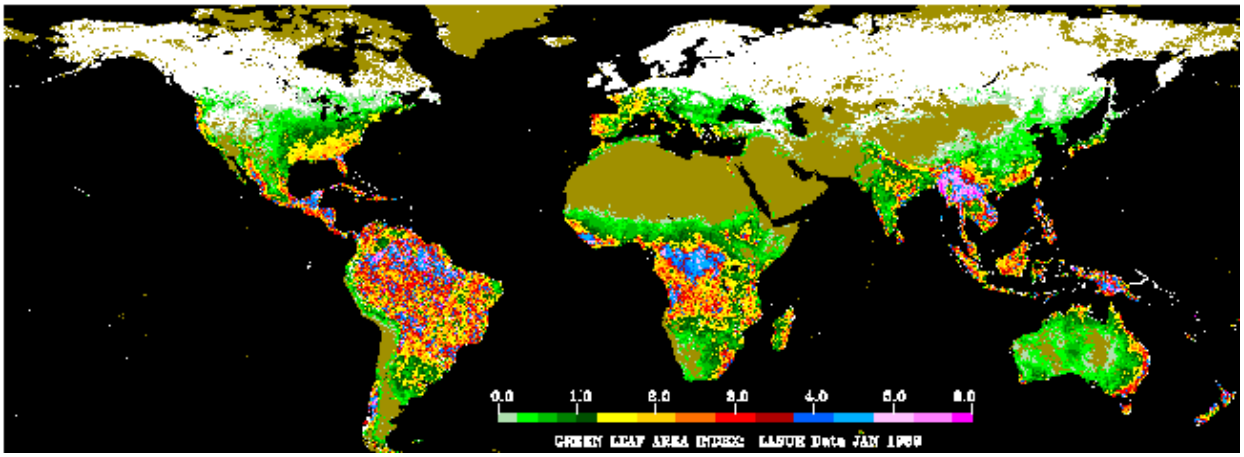

a)

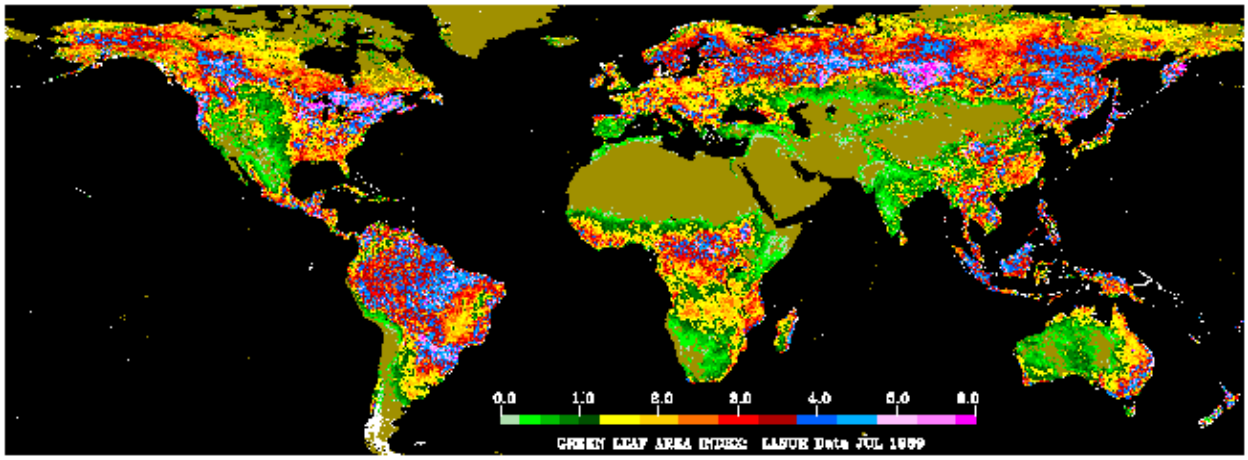

b)

PLATE 2. Global LAI derived from LASUR (LAnd SUrface Reflectance) data. This data set includes atmospherically corrected surface reflectances in the red and near-infrared channels of the Advanced Very High Resolution Radiometer (AVHRR) at global scale (1/7,1, and 5 square degree resolution; one week temporal resolution) for 1989 and 1990. The algorithm was applied to the weekly surface reflectance data (8 km) for 4 weeks in January and for 4 weeks in July. These panels show the color-coded images of global LAI (a) in January and (b) in July composited based on maximum NDVI during those four weeks.

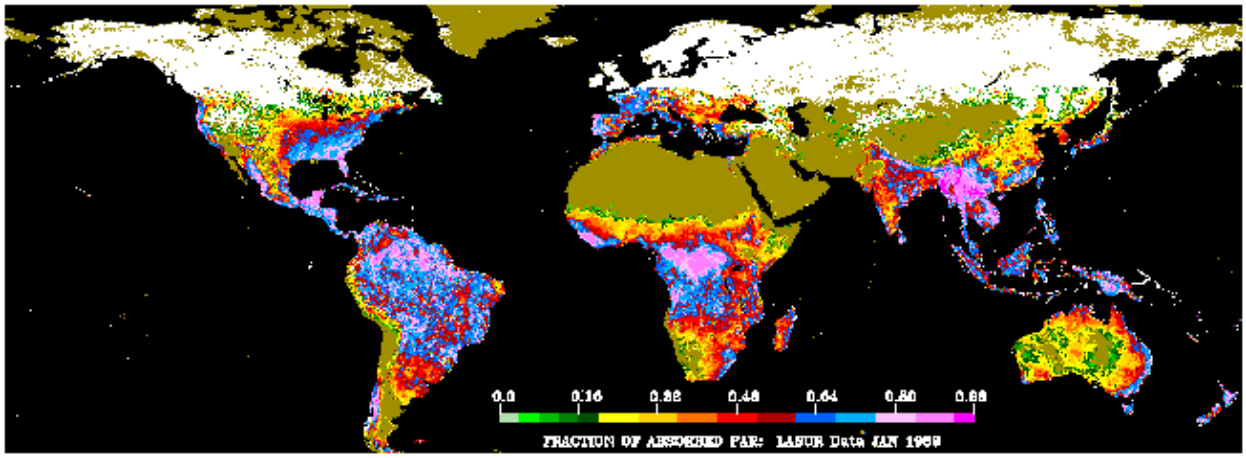

a)

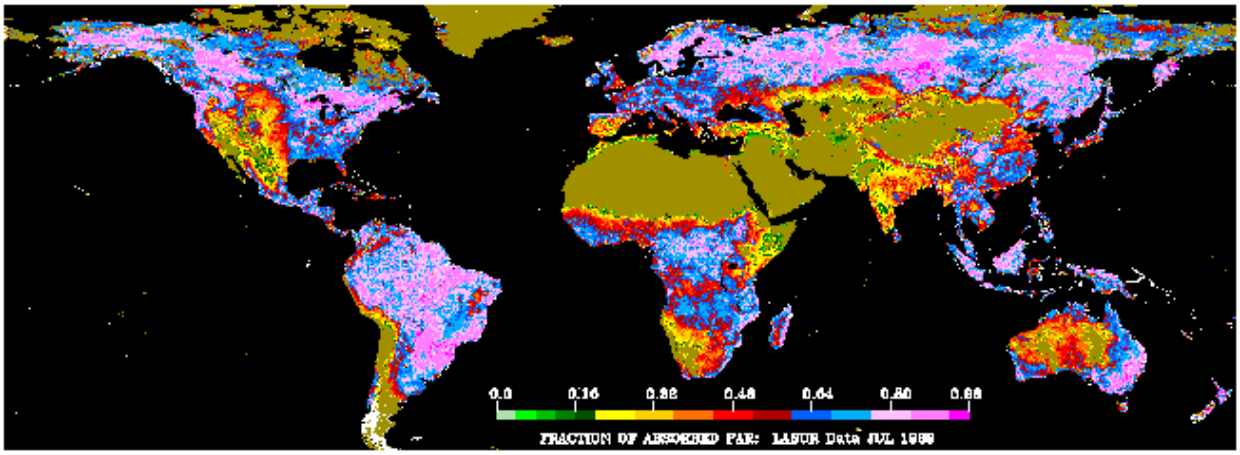

b)

PLATE 3. Global FPAR derived from LASUR data. The algorithm was applied to the weekly surface reflectance data (8 km) for 4 weeks in January and for 4 weeks in July. These panels show the color-coded images of global FPAR in January (a) and in July (b) composited based on maximum NDVI during those four weeks.